**Proceedings of the ASME 2009 International Design Engineering Technical Conferences &
Computers and Information in Engineering Conference
IDETC/CIE 2009
August 30 - September 2, 2009, San Diego, California, USA**

DETC2009-86636

SELF-EXCITED VIBRATIONS IN A DELAY OSCILLATOR: APPLICATION TO MILLING WITH SIMULTANEOUSLY ENGAGED HELICAL FLUTES

Firas A. Khasawneh*
Brian P. Mann
Department of Mechanical Engineering
and Materials Science
Duke University
Durham, North Carolina 27708
Email: firas.khasawneh@duke.edu
brian.mann@duke.edu

Oleg A. Bobrenkov
Eric A. Butcher
Department of Mechanical and
Aerospace Engineering
New Mexico State University
Las Cruces, NM 88003
Email: chaalis@nmsu.edu
eab@nmsu.edu

ABSTRACT

This paper investigates the stability of a milling process with simultaneously engaged flutes by extending the state-space temporal finite elements method. In contrast to prior works, multiple flute engagement due to both a high depth of cut and a high step-over distance are considered. A particular outcome of this study is the development of a frame work to determine the stability of periodic, piecewise continuous delay differential equations. Another major outcome is the demonstration of different stability behavior at the loss of stability in comparison to prior results. To elaborate more, period doubling regions are shown to appear at relatively high radial immersions when multiple flutes with either a zero or non-zero helix angle are simultaneously cutting.

INTRODUCTION

Self-excited vibrations can occur when the forces exciting a system are coupled to the state variables. This coupling can be the result of a feedback mechanism where the excitation forces are a function of current and past state variables. The equations of motion incorporating such mechanism are typically delay differential equations (DDE) which are either autonomous or time-varying. One physical application for DDE is found in metal removal processes. More specifically, many studies have investigated the occurrence of self-excited vibrations in machining, commonly known as chatter.

Chatter is typically characterized by large amplitude oscillations that deteriorate the surface finish and can also damage the tool, machine spindle, and the workpiece. For a limited class of DDEs, e.g. continuous turning, the stability boundaries can be obtained in a closed-form [1]. However, the stability analysis of more general DDEs requires using approximation techniques, such as semi-discretization [2], Chebyshev-based methods [3–5], collocation methods [6], temporal finite element analysis (TFEA) [7–10], as well as frequency domain techniques [11, 12]. Numerical simulation is also used to study machining stability [13–16]; however, semi-analytical predictions of stability can quickly and accurately give stability regions over the process parameter space of interest making them superior to tedious numerical simulations [17–20].

The presence of piecewise continuous coefficients in the DDE considerably increases the level of complexity. Milling, for instance, is a common metal removal process which is commonly approximated as a periodic, piecewise continuous system. Therefore, an approximation scheme, such as TFEA [9, 10, 21–24], is typically necessary to determine milling stability. The stability of milling processes is typically reported through stability diagrams which chart the boundaries between stable and unstable cuts as a function of the spindle speed and depth of cut [25–27].

*Corresponding author

A milling process is stable if it is chatter-free, whereas at the onset of chatter, the process becomes unstable. These diagrams enhance efficiency and reduce costs by eliminating the need for trial and error. In addition to solving for the system stability, semi-analytical techniques can determine the type of bifurcation associated with instabilities.

For example, recent studies have shown that a new bifurcation phenomena can occur in highly intermittent cutting. Besides Neimark-Sacker or secondary Hopf bifurcations, period-doubling bifurcations have been analytically predicted in Refs. [16,18,28,29] and confirmed experimentally in Refs. [22,30–32]; a specific outcome from these works was that they found period-doubling at low radial immersions when only a single tooth was cutting.

A different stability behavior for helical mills was reported and verified experimentally in Refs. [10, 33–35]. Closed boundaries, or islands, of unstable period doubling were shown to appear in the stability diagram due to the helical flutes of the tool. In these works, the period doubling islands were shown only at relatively low radial immersions. Further, Refs. [10, 35] studied the case of only one flute cutting at a time, see Fig. 1-(A), whereas Refs. [33, 34] investigated the case of multiple flutes simultaneously cutting when using a high depth of cut, see Fig. 1-(B). However, the stability analysis for the cases of multiple flutes simultaneously cutting, due to a high step-over distance, (see Fig. 1-(C)), or due to a combination of a high depth of cut and a high step-over distance, see Fig. 1-(D), have not received much attention.

In this paper, we use the state-space TFEA method to study the stability of a milling process. The added complexity of simultaneously engaged flutes for both zero-helix and helical mills is considered. In contrast to prior works, multiple flute engagement due to both a high depth of cut and a high step-over distance are investigated. A particular outcome of this study is the development of a frame work to determine the stability of DDEs with periodic discontinuities in a parameter. Another major outcome is the demonstration of a different stability behavior at the loss of stability in comparison to prior results. To elaborate more, period doubling regions are shown to appear at relatively high radial immersions when multiple flutes with either a zero or non-zero helix angle are cutting simultaneously.

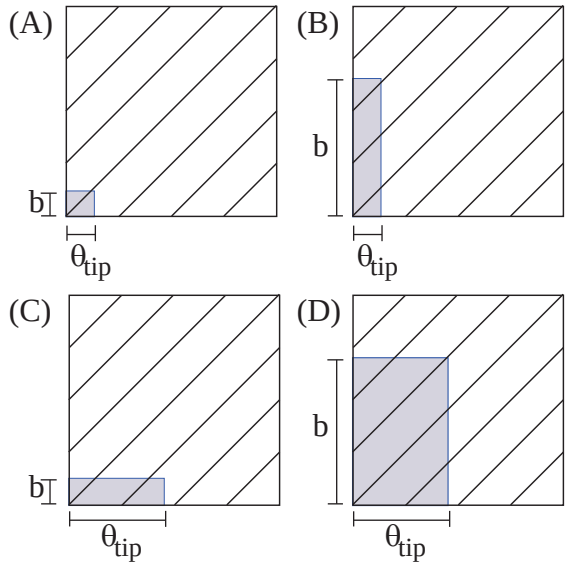

Figure 1. THE DIFFERENT CASES ASSOCIATED WITH A HELICAL MILLING TOOL. THE GRAY AREA REPRESENTS THE CUTTING ZONE AND IN GRAPH (A), ONLY A SINGLE FLUTE IS CUTTING AT ANY INSTANT, WHILE IN GRAPHS (B) AND (C) MULTIPLE FLUTES ARE CUTTING DUE TO A HIGH DEPTH OF CUT, AND A HIGH RADIAL STEP-OVER DISTANCE, RESPECTIVELY. GRAPH (D) SHOWS THE CASE OF A HIGH DEPTH OF CUT COMBINED WITH A HIGH RADIAL STEP-OVER DISTANCE. THE VARIABLES SHOWN IN THE FIGURE ARE DEFINED IN THE MECHANICAL MODEL SECTION.

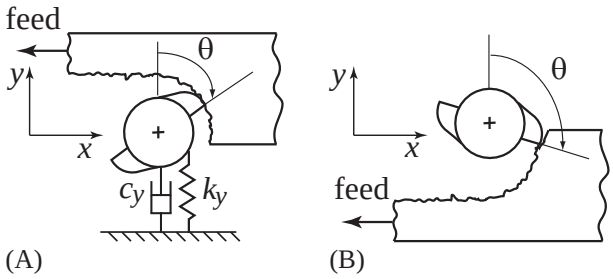

Figure 2. ILLUSTRATIONS OF (A) UP-MILLING, AND (B) DOWN-MILLING.

Mechanical Model

The equation of motion (EOM) for a single-mode helical mill compliant only in the y direction such as the one shown in Fig. 2, (or similarly for a workpiece compliant in the y direction), is described by

$$\ddot{y}(t) + 2\zeta\omega_{\rm n}\dot{y}(t) + \omega_{\rm n}^2 y(t) = \frac{1}{m_y} F_y(z,t,\tau), \qquad (1)$$

where m_y, $\omega_{\rm n}$, and ζ are the modal mass, natural frequency and damping ratio, respectively. The term $F_y(z,t,\tau)$ describes the cutting forces in the y-direction while the time delay $\tau = 2\pi/N\Omega$ is the tooth passage period for an N-tooth cutter rotating at a spindle speed Ω (rad/sec). An analytical expression for F_y can be obtained by first introducing the differential forces, shown

in Fig. 3, in the tangential and radial directions [36] according to

$$dF_t = K_t w\left(\theta_n(t,z),\tau\right)\, dz, \tag{2a}$$
$$dF_r = K_r w(\theta_n(t,z),\tau)\, dz, \tag{2b}$$

where K_t and K_r are the tangential and radial specific cutting force coefficients, respectively, and the variable z varies along the axial direction of the tool from 0 at the tip to b—the depth of cut. The angle $\theta_n(t,z)$ describes the rotation angle of the n^{th} flute from the vertical reference shown in Fig. 2, and is described by

$$\theta_n(t,z) = \Omega t - (n-1)\theta_{\rm p} - \kappa z, \qquad \text{where } n = 1,2,\ldots,N \tag{3}$$

where $\theta_{\rm p}$ is the tool pitch angle, i.e. $\theta_{\rm p} = 2\pi/N$ for a tool with uniformly spaced flutes, and $\kappa = 2\tan\beta/D$ is a helix parameter. The radial chip thickness for the reference cutting tooth can be found by applying the circular tool path assumption which yields [37, 38]

$$w(\theta_n(t,z)) = h\sin(\theta_n(t,z)) + [y(t) - y(t-\tau)]\cos(\theta_n(t,z)), \tag{4}$$

where h is the feed per tooth. The total force in the y direction is found by integrating Eqs. (2a) and (2b) with respect to the differential axial depth dz which gives

$$F_y = g_n(t) \int_{z_a(n,t)}^{z_b(n,t)} \left[\frac{dF_t}{dz}\sin\theta_n(t,z) - \frac{dF_r}{dz}\cos\theta_n(t,z)\right] dz, \tag{5}$$

where $g_n(t)$ is a switching function: its value is 1 if the n^{th} tooth is cutting, and 0 if the tooth exits the cut. The functions $z_a(n,t)$ and $z_b(n,t)$ describe the lower and upper limits of integration, respectively, and they are graphed in Fig. 4 where they are shown to vary according to

$$z_a(n,t) = \begin{cases} 0 & \text{if } \theta_{\rm st} \le \theta_n \le \theta_{\rm st} + \theta_{\rm tip}, \\ \frac{\theta_n - (\theta_{\rm st} + \theta_{\rm tip})}{\kappa} & \text{if } \theta_{\rm st} + \theta_{\rm tip} < \theta_n, \end{cases} \tag{6a}$$

$$z_b(n,t) = \begin{cases} \frac{\theta_n - \theta_{\rm st}}{\kappa} & \text{if } \theta_{\rm st} \le \theta_n \le \theta_{\rm st} + \theta_{\rm lag}, \\ b & \text{if } \theta_{\rm st} + \theta_{\rm lag} < \theta_n, \end{cases} \tag{6b}$$

where $\theta_{\rm tip}$ is the angular distance over which the tool is cutting, $\theta_{\rm st}$ is the entry angle which is 0 for up-milling and $\pi - \theta_{\rm tip}$ for down-milling, while $\theta_{\rm lag} = \kappa b$ is the angular distance defined in Fig. 3.

The angular distance, $\theta_{\rm tip}$, depends on the ratio of the radial step-over distance to the tool diameter, which is often called the radial immersion (RI), according to

$$\theta_{\rm tip} = \cos^{-1}(1 - 2{\rm RI}). \tag{7}$$

Substituting the expression for the total force in the y direction, Eq. (5), into Eq. (1), the equation of motion now reads

$$\ddot{y}(t) + 2\zeta\omega_{\rm n}\dot{y}(t) + \omega_{\rm n}^2 y(t) = \frac{K_c(t,b)}{m_y}(y(t) - y(t-\tau)), \tag{8}$$

where only the dynamic chip thickness was considered, i.e. by ignoring the term $h\sin\theta_n(t,z)$ in Eq. (4) which does not affect the stability analysis. The directional force coefficient $K_c(t,b)$ is τ-periodic and is a function of time and the depth of cut b [34,35].

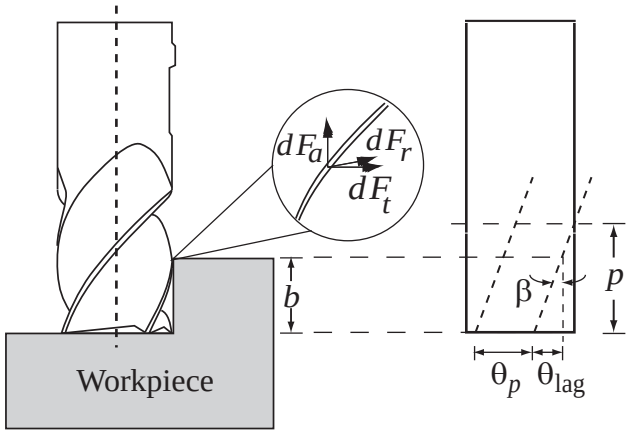

Figure 3. SCHEMATIC OF A HELICAL END MILL WITH MULTIPLE FLUTES AS WELL AS THE DIFFERENTIAL CUTTING FORCES IN THE AXIAL, RADIAL, AND TANGENTIAL DIRECTIONS.

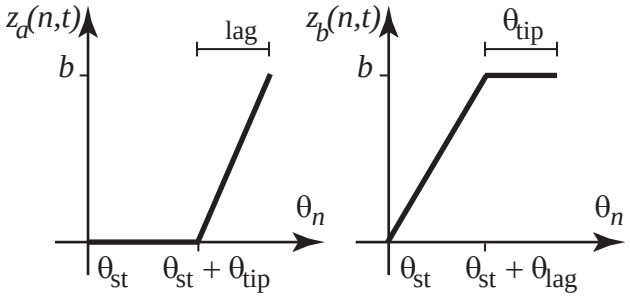

Figure 4. A PLOT OF THE INTEGRATION LIMITS DESCRIBED IN EQS. (6) AS A FUNCTION OF THE FLUTE ROTATION ANGLE

This coefficient is defined using Eqs. (2a), (2b) and (4) as follows

$$K_c(t,b) = \sum_{n=1}^{N_t} g_n(t) \int_{z_a(n,t)}^{z_b(n,t)} (K_t \sin\theta_n \cos\theta_n - K_r \cos^2\theta_n)\, dz, \tag{9}$$

where the summation is over the the total number of simultaneously engaged flutes $N_t = \lceil (\theta_{tip} + \theta_{lag})/\theta_p \rceil$, where $\lceil \cdot \rceil$ is the ceiling function.

It is necessary here to make a distinction between the tool pitch angle θ_p and the mill helix pitch p which are related according to $\theta_p = \kappa p$. Whereas the pitch angle describes the angular distance between two consecutive teeth, the mill helix pitch describes the distance between two adjacent flutes along the axis of the tool, as shown in Fig. 3. Further, the mill helix pitch is a geometric property of helixes, and it is given mathematically by [33]

$$p = \frac{D\pi}{N \tan\beta}, \tag{10}$$

where D is the diameter of the tool and β is the helix angle defined in Fig. 3. Both θ_p and p play an important role in determining whether multiple flutes are cutting or not. Specifically, the condition for multiple flutes in contact is $\lceil (\theta_{tip} + \theta_{lag})/\theta_p \rceil > 1$, see Fig. 1.

In the next section, the discretization technique known as temporal finite element analysis (TFEA) is used to study the stability of Eq. (8).

STABILITY ANALYSIS USING TFEA

This section describes the steps involved in using TFEA to determine the stability of Eq. (8). The results of the stability analysis are then presented in a series of charts that show the stability boundaries as a function of the process parameters, namely, the spindle speed and the depth of cut.

In order to use the state-space TFEA method, Eq. (8) is first re-written in its state-space form

$$\frac{d\mathbf{y(t)}}{dt} = \mathbf{A}\,\mathbf{y}(t) + \mathbf{B}\,\mathbf{y}(t-\tau), \tag{11}$$

where the state vectors and the state matrices are

$$\mathbf{y}(t) = \begin{bmatrix} y(t) & \dot{y}(t) \end{bmatrix}^{\mathrm{T}}, \tag{12a}$$

$$\mathbf{y}(t-\tau) = \begin{bmatrix} y(t-\tau) & \dot{y}(t-\tau) \end{bmatrix}^{\mathrm{T}}, \tag{12b}$$

$$\mathbf{A} = \begin{bmatrix} 0 & 1 \\ -\omega_n^2 + \frac{Kc(t,b)}{m_y} & -2\zeta\,\omega_n \end{bmatrix}, \tag{12c}$$

$$\mathbf{B} = \begin{bmatrix} 0 & 0 \\ -\frac{Kc(t,b)}{m_y} & 0 \end{bmatrix}. \tag{12d}$$

The solution vector $\mathbf{y}(t)$ is then approximated as a linear combination of polynomials during the j^{th} element according to

$$\mathbf{y}(t) = \sum_{i=1}^{3} \mathbf{a}_{ji}\phi_i(\sigma), \tag{13a}$$

$$\mathbf{y}(t-\tau) = \sum_{i=1}^{3} \mathbf{a}_{(j-E,i)}\phi_i(\sigma), \tag{13b}$$

where j is the element index, σ is the local element time, E is the number of elements used, t_j is the length of the j^{th} element, and ϕ_i is the i^{th} trial function. For this analysis, the set of polynomial trial functions used is

$$\phi_1(\sigma) = 1 - 23(\frac{\sigma}{t_j})^2 + 66(\frac{\sigma}{t_j})^3 - 68(\frac{\sigma}{t_j})^4 + 24(\frac{\sigma}{t_j})^5, \tag{14a}$$

$$\phi_2(\sigma) = 16(\frac{\sigma}{t_j})^2 - 32(\frac{\sigma}{t_j})^3 + 16(\frac{\sigma}{t_j})^4, \tag{14b}$$

$$\phi_3(\sigma) = 7(\frac{\sigma}{t_j})^2 - 34(\frac{\sigma}{t_j})^3 + 52(\frac{\sigma}{t_j})^4 - 24(\frac{\sigma}{t_j})^5. \tag{14c}$$

These vectors represent an approximate solution for Eq. (11) in the form of a linear combination of the trial functions ϕ_i. The local time, σ, varies from zero to t_j—the time of each element. The chosen trial functions are orthogonalized on the interval $0 \le \sigma \le t_j$ and the use of the local time notation ensures that they also remain orthogonal for every temporal element. These functions are obtained through interpolation, and they are constructed such that the coefficients of the assumed solution directly represent the state variable at the beginning, middle and end of each temporal element, i.e. at $\sigma = 0$, $t_j/2$ and t_j, respectively. The construction and properties of these functions are discussed in more details in Ref. [39].

Substituting the expressions of Eq. (13) into Eq. (11) gives

$$\sum_{i=1}^{3} \mathbf{a}_{ji}\dot{\phi}_i(\sigma) = \mathbf{A}(t_e)\sum_{i=1}^{3} \mathbf{a}_{ji}\phi_i(\sigma) + \mathbf{B}(t_e)\sum_{i=1}^{3} \mathbf{a}_{(j-E,i)} + \text{error}, \tag{15}$$

where $t_e = \sigma + (j-1)t_j$ and the error is induced by the approximation procedure. To reduce this error, the method of weighted residuals is applied through multiplying Eq. (15) by independent weight functions, integrating over the length of one element, and setting the resulting error term to zero which yields

$$\int_0^{t_j} \sum_{i=1}^{3} \mathbf{a}_{ji}\dot{\phi}_i(\sigma)\psi_p(\sigma)\,d\sigma = \int_0^{t_j} \mathbf{A}(t_e) \sum_{i=1}^{3} \mathbf{a}_{ji}\phi_i(\sigma)\psi_p(\sigma)\,d\sigma + \int_0^{t_j} \mathbf{B}(t_e) \sum_{i=1}^{3} \mathbf{a}_{(j-E,i)}\ \phi_i(\sigma)\psi_p(\sigma)\,d\sigma, \quad (16)$$

where ψ_p are the weight functions. In this study, the shifted Legendre polynomials $\psi_1(\sigma) = 1$ and $\psi_2(\sigma) = 2(\sigma/tj) - 1$ were used. Rearranging the terms of Eq. (16), it can be rewritten as

$$\sum_{i=1}^{3} \mathbf{C}^p_{ji}\mathbf{a}_{ji} = \sum_{i=1}^{3} \mathbf{D}^p_{ji}\mathbf{a}_{(j-E,i)}, \quad (17)$$

where the above matrices are defined as

$$\mathbf{C}^p_{ji} = \int_0^{t_j} \left(\mathbf{I}\dot{\phi}_i(\sigma) - \mathbf{A}(t_e)\phi_i(\sigma)\right)\psi_p(\sigma)\,d\sigma, \quad (18a)$$

$$\mathbf{D}^p_{ji} = \int_0^{t_j} \mathbf{B}(t_e)\phi_i(\sigma)\psi_p(\sigma)\,d\sigma, \quad (18b)$$

and $\mathbf{I}$ is an identity matrix. Using Eq. (18), a global matrix can be constructed according to

$$\mathbf{H}\,\mathbf{a}_\tau = \mathbf{G}\,\mathbf{a}_{-\tau}, \quad (19)$$

where $\mathbf{a}_\tau$ and $\mathbf{a}_{-\tau}$ are the coefficients of the approximate solution in the current and the previous period, respectively. Assuming $E = 2$ for demonstration as shown in Fig. 5, elements 1 and 2 are mapped onto elements 3 and 4 and the expressions for $\mathbf{H}$ and $\mathbf{G}$ become

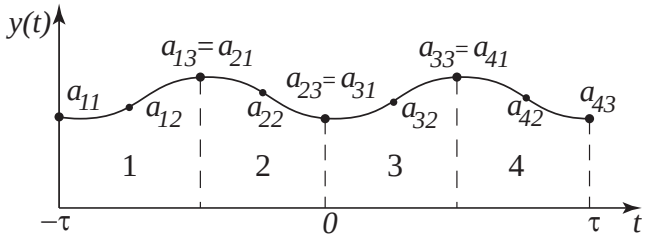

Figure 5. TFEA TIME LINE. TWO ELEMENTS ARE USED IN EACH PERIOD FOR DEMONSTRATION.

$$\mathbf{H} = \begin{bmatrix} \mathbf{I} & 0 & 0 & 0 & 0 \\ \mathbf{C}^1_{31} & \mathbf{C}^1_{32} & \mathbf{C}^1_{33} & 0 & 0 \\ \mathbf{C}^2_{31} & \mathbf{C}^2_{32} & \mathbf{C}^2_{33} & 0 & 0 \\ 0 & 0 & \mathbf{C}^1_{41} & \mathbf{C}^1_{42} & \mathbf{C}^1_{43} \\ 0 & 0 & \mathbf{C}^2_{41} & \mathbf{C}^2_{42} & \mathbf{C}^2_{43} \end{bmatrix}, \quad (20a)$$

$$\mathbf{G} = \begin{bmatrix} 0 & 0 & 0 & 0 & \mathbf{\Phi} \\ \mathbf{D}^1_{11} & \mathbf{D}^1_{12} & \mathbf{D}^1_{13} & 0 & 0 \\ \mathbf{D}^2_{11} & \mathbf{D}^2_{12} & \mathbf{D}^2_{13} & 0 & 0 \\ 0 & 0 & \mathbf{D}^1_{21} & \mathbf{D}^1_{22} & \mathbf{D}^1_{23} \\ 0 & 0 & \mathbf{D}^2_{21} & \mathbf{D}^2_{22} & \mathbf{D}^2_{23} \end{bmatrix}, \quad (20b)$$

where $\mathbf{\Phi}$ is the state transition matrix

$$\mathbf{\Phi} = \frac{1}{\lambda_1 - \lambda_2} \begin{bmatrix} \lambda_1 e^{\lambda_2 t_f} - \lambda_2 e^{\lambda_1 t_f} & e^{\lambda_1 t_f} - e^{\lambda_2 t_f} \\ \lambda_1\lambda_2 e^{\lambda_2 t_f} - \lambda_1\lambda_2 e^{\lambda_1 t_f} & \lambda_1 e^{\lambda_1 t_f} - \lambda_2 e^{\lambda_2 t_f} \end{bmatrix}, \quad (21)$$

and $\lambda_{1,2} = \zeta \pm \sqrt{\zeta^2 - 1}$, while t_f is the duration of free vibration. This state transition matrix relates the state of the tool as it exits the cut to its state as it re-enters the cut [40].

Recalling that the coefficients of the assumed solution directly represent the state variable at various points in time, Eq. (19) can be alternatively written as

$$\mathbf{y}_\tau = \mathbf{Q}\,\mathbf{y}_{-\tau}, \quad (22)$$

where $\mathbf{Q} = \mathbf{H}^{-1}\mathbf{G}$ is called the monodromy operator. Equation (22) represents a discrete solution form for Eq. (8) that maps the states of the system over one delay period τ. The condition for asymptotical stability requires that all the characteristic multipliers, or eigenvalues of $\mathbf{Q}$, must lie within the unit circle in the complex plane. More details about this technique and its convergence properties can be found in Ref. [39].

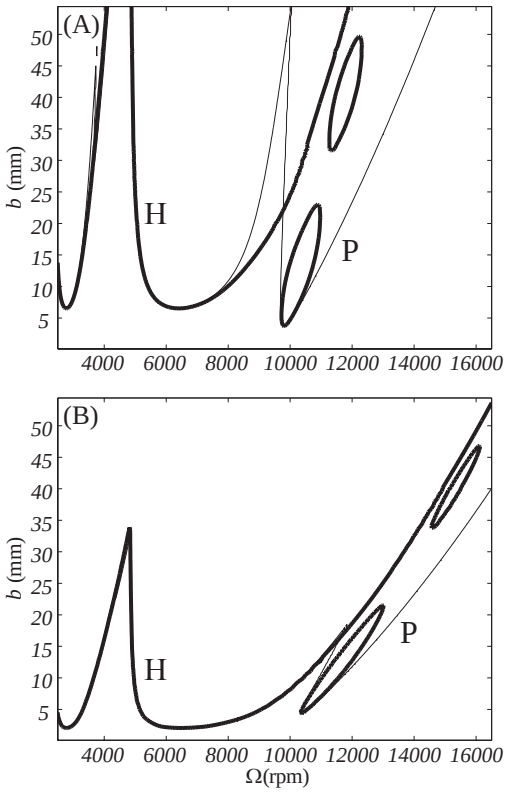

Figure 6. DOWN-MILLING STABILITY DIAGRAMS OF EQ. (8) FOR A 4-FLUTE CUTTER. THE LIGHT LINE REPRESENTS THE ZERO HELIX CASE WHILE THE THICK LINE REPRESENTS A HELICAL TOOL WITH $\beta = 30$. THE PARAMETERS USED TO GENERATE THE PLOTS ARE SHOWN IN TABLE 1 AND THE RADIAL IMMERSIONS USED ARE (A) 0.05, AND (B) 0.50. "H" INDICATES HOPF BIFURCATIONS, WHILE "P" INDICATES PERIOD-DOUBLING BIFURCATIONS.

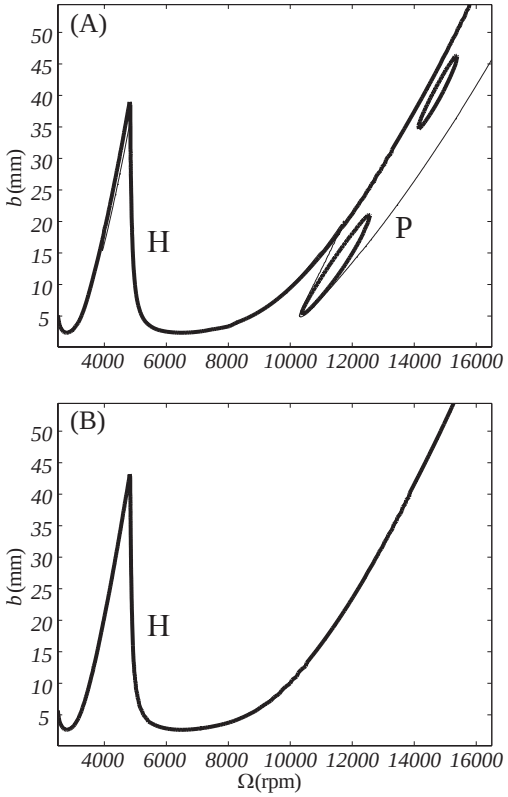

Figure 7. DOWN-MILLING STABILITY DIAGRAMS OF EQ. (8) FOR A 4-FLUTE CUTTER. THE LIGHT LINE REPRESENTS THE ZERO HELIX CASE WHILE THE THICK LINE REPRESENTS A HELICAL TOOL WITH $\beta = 30$. THE PARAMETERS USED TO GENERATE THE PLOTS ARE SHOWN IN TABLE 1 AND THE RADIAL IMMERSIONS USED ARE (A) 0.75, AND (B) 1.0 (FULL RADIAL IMMERSION). "H" INDICATES HOPF BIFURCATIONS, WHILE "P" INDICATES PERIOD-DOUBLING BIFURCATIONS.

Discussion and Results

The results from the stability analysis for a milling process are given in this section. The process is described by Eq. (15) and the cases studied are for multi-flute cutters with and without a helix angle. Although the stability analysis approach described earlier can be used to study both up-milling and down-milling processes, see Fig. 2, only the down-milling cases, shown in Figs. 6–9, were considered in this study.

The parameters used to obtain these plots were introduced in Refs. [33, 34] and are shown in Tab. 1. The results for both a zero-helix mill (light line), and a helical mill with $\beta = 30^o$ (dark line) are reported in each diagram. The type of bifurcation is also marked on each lobe with "H" indicating a Neimark-Sacker or Hopf bifurcation, and "P" indicating period doubling lobes. The authors acknowledge that changing the geometry of the tool would in general change the specific cutting coefficients K_r and K_t. Therefore, a one to one stability comparison between a zero-helix tool and helical one would require accounting for these changes. However, we are primarily interested in the island phenomena associated with helical mills and the zero-helix cases are only given for reference.

In Fig. 6-(A), a radial immersion of 0.05 was used which produced identical results to those obtained through a frequency domain stability analysis in Ref. [34]. This case corresponds to graphs (A) and (B) in Fig. 1, where incrementing the depth of cut to high values results in multiple-flute engagement. It can be seen that the period doubling boundary, which corresponds to the zero-helix case, transforms into closed, bounded regions of period doubling that are often called islands. The depths of cut at the period-doubling free zones between any two islands correspond to integer multiples of the helix pitch. This is because at these values of cutting depths the helical flutes average the time-periodic forces and the system becomes autonomous [33].

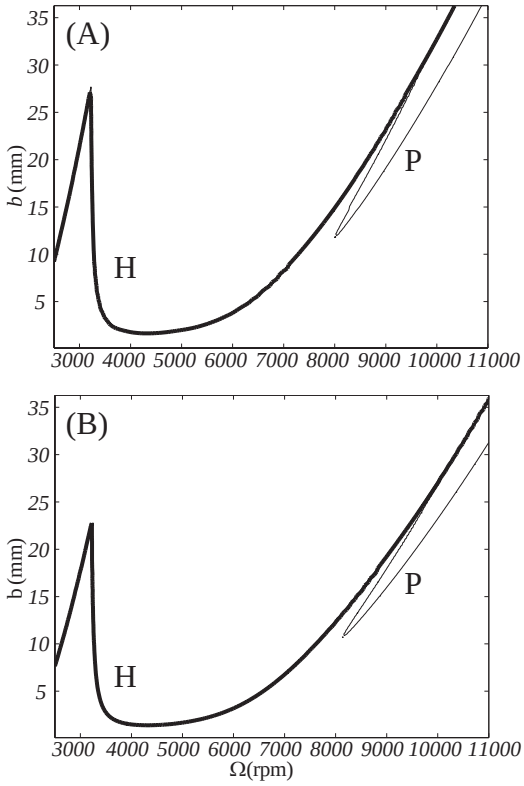

Figure 8. DOWN-MILLING STABILITY DIAGRAMS OF EQ. (8) FOR A 6-FLUTE CUTTER. THE LIGHT LINE REPRESENTS THE ZERO HELIX CASE WHILE THE THICK LINE REPRESENTS A HELICAL TOOL WITH $\beta = 30$. THE PARAMETERS USED TO GENERATE THE PLOTS ARE SHOWN IN TABLE 1 AND THE RADIAL IMMERSIONS USED ARE (A) 0.25, AND (B) 0.50. "H" INDICATES HOPF BIFURCATIONS, WHILE "P" INDICATES PERIOD-DOUBLING BIFURCATIONS.

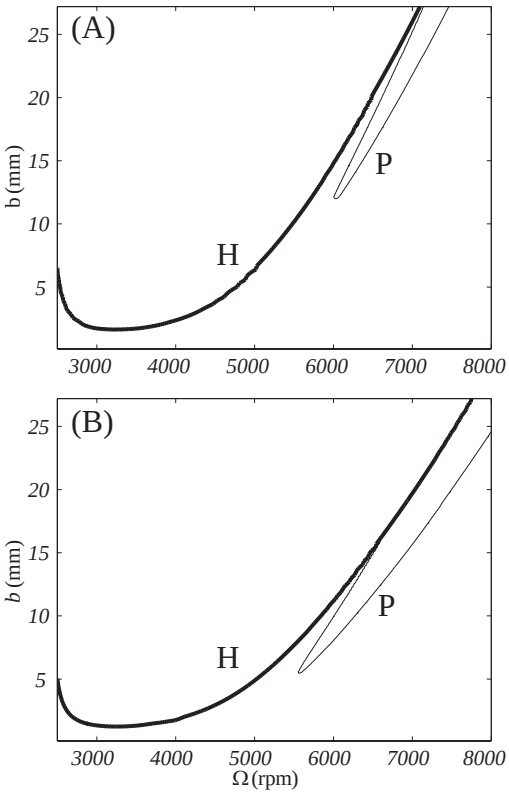

Figure 9. DOWN-MILLING STABILITY DIAGRAMS OF EQ. (8) FOR AN 8-FLUTE CUTTER. THE LIGHT LINE REPRESENTS THE ZERO HELIX CASE WHILE THE THICK LINE REPRESENTS A HELICAL TOOL WITH $\beta = 30$. THE PARAMETERS USED TO GENERATE THE PLOTS ARE SHOWN IN TABLE 1 AND THE RADIAL IMMERSIONS USED ARE (A) 0.146, AND (B) 0.25. "H" INDICATES HOPF BIFURCATIONS, WHILE "P" INDICATES PERIOD-DOUBLING BIFURCATIONS.

The radial immersion is increased to 0.50 in Fig. 6-(B); this is the borderline case for only one flute in the cut when using a zero-helix mill and four cutting flutes. The period doubling lobes for the zero-helix case and the islands for the helical tool case are still apparent at this radial immersion. However, in contrast to prior works on a single flute in the cut, a further increase of the radial immersion in Fig. 7-(A) to 0.75 causes multiple flute engagement for the zero-helix case and produces cases similar to those depicted in Fig. 1-(C) and (D) for a helical tool. The appearance of period-doubling lobes at this relatively high radial immersion diverges from the stability behavior for a single flute. The period doubling regions disappear at full radial immersion, see Fig. 7-(B), and the results for zero-helix and helical tools become identical under the assumption of constant specific cutting coefficients.

The cases for a 6-flute and an 8-flute cutter demonstrate a different behavior as shown in Figs. 8 and 9, respectively. For example, in Fig. 8, period doubling regions still appear for the zero-helix case at both the borderline case for only one flute in the cut, graph (A), as well as the case with a higher radial immersion and a zero-helix mill in graph (B). However, when a helical mill is used, the period doubling lobes disappear and only Neimark-Sacker lobes persist. The same observation is apparent in graphs (A) and (B) in Fig. 9 for an 8-flute cutter; whereas period doubling lobes appear for the zero-helix case, only Neimark-Sacker lobes appear for the helical tool cases. This is because as the number of teeth is increased, the spacing between the helical flutes gets smaller—decreasing both the pitch angle and the helix pitch. The forces are therefore averaged out around the tool helix over the full range of cutting speeds and depths of cut. The smoothing effect of the helix angle asymptotically transforms a discontinuous milling process into a continuous one as the number of flutes is increased. Hence, when a sufficient number of cutting edges is used, only Neimark-Sacker bifurcations appear.

Conclusions

This paper presented an approach to solve for the stability of DDE with piecewise discontinuities. The method used was the state-space TFEA and the physical application under consideration was a single degree of freedom milling process with simultaneously cutting flutes. The stability charts for both a zero-helix mill and a helical tool were shown and compared under the assumption of constant specific cutting coefficients. It was shown that the state-space TFEA results agreed with the frequency domain stability results for the low radial immersion cases found in literature. However, increasing the radial immersion beyond the range investigated in literature revealed a different stability.

In contrast to prior works, period doubling regions appeared at relatively high radial immersions when multiple flutes were cutting. These regions appeared as lobes for zero-helix tools, while closed islands characterized the period doubling regions for helical tools. However, as the number of cutting edges is increased, e.g. to 6 and 8 in Figs. 8 and 9, the helical flutes smoothed out the force discontinuities and eliminated period doubling bifurcations.

Additionally, in agreement with prior works, period doubling bifurcations were shown to cease to exist at depths of cut equal to integer multiples of the mill helix pitch. Moreover, at full slotting, only Neimark-Sacker bifurcations existed and the results for zero-helix and helical tools coincided.

Although only Neimark-Sacker and period doubling bifurcations can occur for tools with constant helix angle and constant pitch, a recent study has found cyclic-fold bifurcations at low radial immersions for both variable pitch and variable helix tools [41]. However, expanding the approach of this paper to the cases of variable pitch and variable helix tools remains a topic for future research.

Table 1. THE PARAMETERS USED TO GENERATE THE STABILITY PLOTS IN FIGS. 6 AND 7.

Parameter	value
m (Kg)	5.3640
ω_{n} (Hz)	319.375
ζ	0.0196
K_t (N/mm^2)	804.3
K_r (N/mm^2)	331

ACKNOWLEDGMENT

Support from US National Science Foundation Grant No. 0114500, and CAREER Award (CMMI-0757776) is gratefully acknowledged.

REFERENCES

[1] Stépán, G., 1989. *Retarded Dynamical Sytems: Stability and Characteristic Functions*. John Wiley & Sons.

[2] Insperger, T., and Stépán, G., 2004. "Updated semi-discretization method for periodic delay-differential equations with discrete delay". *International Journal for Numerical Methods,* **61**, pp. 117–141.

[3] Ma, H., Butcher, E. A., and Bueler, E., 2003. "Chebyshev expansion of linear and piecewise linear dynamic systems with time delay and periodic coefficients under control excitations". *Journal of Dynamic Systems, Measurement, and Control,* **125**, pp. 236–243.

[4] Butcher, E. A., Ma, H., Bueler, E., Averina, V., , and Szabó, Z., 2004. "Stability of linear time-periodic delay-differential equations via Chebyshev polynomials". *International Journal Numerical Methods in Engineering,* **59**, pp. 895–922.

[5] V. Deshmukh, H. M., and Butcher, E. A., 2006. "Optimal control of parametrically excited linear delay differential systems via Chebyshev polynomials". *Optimal Control Applications and Methodology,* **27**, pp. 123–136.

[6] Engelborghs, K., Luzyanina, T., in T Hout, K. J., and Roose, D., 2000. "Collocation methods for the computation of periodic solutions of delay differential equations". *SIAM J. Sci. Comput.,* **22**, pp. 1593–1609.

[7] Argyris, J. H., and Scharpf, D. W., 1969. "Finite elements in time and space". *Aeronautical Journal of the Royal Society,* **73**, pp. 1041–1044.

[8] Borri, M., Bottasso, C., and Mantegazza, P., 1992. "Basic features of the time finite element approach for dynamics". *Meccanica,* **27**, pp. 119–130.

[9] Mann, B. P., Garg, N. K., Young, K. A., and Helvey, A. M., 2005. "Milling bifurcations from structural asymmetry and nonlinear regeneration". *Nonlinear Dynamics,* **42**(4), pp. 319–337.

[10] Patel, B. R., Mann, B. P., and Young, K. A., 2008. "Uncharted islands of chatter instability in milling". *International Journal of Machine Tools and Manufacture,* **48**, pp. 124–134.

[11] Budak, E., and Altintas, Y., 1998. "Analytical prediction of chatter stability conditions for multi-degree of systems in milling. part i: Modelling". *Journal of Dynamic Systems, Measurement and Control,* **120**, pp. 22–30.

[12] Merdol, S. D., and Altintas, Y., 2004. "Multi frequency solution of chatter stability for low immersion milling". *Jour-*

nal of Manufacturing Science and Engineering, **126**(3), pp. 459–466.

[13] Schmitz, T., Davies, M., Medicus, K., and Snyder, J., 2001. "Improving high-speed machining material removal rates by rapid dynamic analysis". *CIRP ANNALS-MANUFACTURING TECHNOLOGY,* **50**(1), pp. 263–268.

[14] Smith, S., and Tlusty, J., 1991. "An overview of the modeling and simulation of the milling process". *Journal of Engineering for Industry,* **113**, pp. 169–175.

[15] Montgomery, D., and Altintas, Y., 1991. "Mechanism of cutting force and surface generation in dynamic milling". *Journal of Engineering for Industry,* **113**, pp. 160–168.

[16] Zhao, M. X., and Balachandran, B., 2001. "Dynamics and stability of milling process". *International Journal of Solids and Structures,* **38**(10–13), pp. 2233–2248.

[17] Altintas, Y., and Budak, E., 1995. "Analytical prediction of stability lobes in milling". *CIRP Annals,* **44**(1), pp. 357–362.

[18] Davies, M. A., Pratt, J. R., Dutterer, B., and Burns, T. J., 2002. "Stability prediction for low radial immersion milling". *Journal of Manufacturing Science and Engineering,* **124**(2), pp. 217–225.

[19] Minis, I., and Yanushevsky, R., 1993. "A new theoretical approach for prediction of machine tool chatter in milling". *Journal of Engineering for Industry,* **115**, pp. 1–8.

[20] Insperger, T., and Stépán, G., 2000. "Stability of the milling process". *Periodica Polytechnica,* **44**(1), pp. 47–57.

[21] Mann, B. P., Bayly, P. V., Davies, M. A., and Halley, J. E., 2004. "Limit cycles, bifurcations, and accuracy of the milling process". *Journal of Sound and Vibration,* **277**, pp. 31–48.

[22] Insperger, T., Mann, B. P., Stépán, G., and Bayly, P. V., 2003. "Stability of up-milling and down-milling, part 1: Alternative analytical methods". *International Journal of Machine Tools and Manufacture,* **43**, pp. 25–34.

[23] Mann, B. P., Young, K. A., Schmitz, T. L., and Dilley, D. N., 2005. "Simultaneous stability and surface location error predictions in milling". *J. Manufacturing Science and Engineering,* **127**, pp. 446–453.

[24] Schmitz, T., and Mann, B., 2006. "Closed form solutions for the prediction of surface location error in milling". *International Journal of Machine Tools and Manufacture,* **46**, pp. 1369–1377.

[25] Tobias, S. A., 1965. *Machine Tool Vibration*. Blackie, London.

[26] Tlusty, J., and Polacek, M., 1963. "The stability of machine tools against self-excited vibrations in machining". In Proceedings of the ASME International Research in Production Engineering, pp. 465–474.

[27] Merrit, H. E., 1965. "Theory of self-excited machine-tool chatter". *Journal of Engineering for Industry,* **87**(4), pp. 447–454.

[28] Davies, M. A., Pratt, J. R., Dutterer, B., and Burns, T. J., 2000. "The stability of low immersion milling". *Annals of the CIRP,* **49**, pp. 37–40.

[29] Bayly, P. V., Halley, J. E., Mann, B. P., and Davis, M. A., 2003. "Stability of interrupted cutting by temporal finite element analysis". *Journal of Manufacturing Science and Engineering,* **125**, May, pp. 220–225.

[30] Insperger, T., Stepan, G., Bayly, P. V., and Mann, B. P., 2003. "Multiple chatter frequencies in milling processes". *Journal of Sound and Vibration,* **262**(2), pp. 333–345.

[31] Mann, B. P., Insperger, T., Bayly, P. V., and Stépán, G., 2003. "Stability of up-milling and down-milling, part 2: Experimental verification". *International Journal of Machine Tools and Manufacture,* **43**, pp. 35–40.

[32] Balachandran, B., 2001. "Non-linear dynamics of milling process". *Proceedings of the Royal Society of London A,* **359**, pp. 793–819.

[33] Insperger, T., Muñoa, J., Zatarain, M., and Peigné, G., 2006. "Unstable islands in the stability chart of milling processes due to the helix angle". In Proceedings of CIRP second International Conference on High Performance Cutting, Vancouver, Canada, CIRP.

[34] Insperger, T., Muñoa, J., Zatarain, M., and Peigné, G., 2006. "Analysis of the influence of mill helix angle on chatter stability". *Annals of CIRP,* **55**.

[35] Mann, B. P., Edes, B. T., Easley, S. J., Young, K. A., and Ma, K., 2008. "Chatter vibration and surface location error prediction for helical end mills". *International Journal of Machine Tools and Manufacture,* **48**, pp. 350–361.

[36] Altintaş, Y., 2000. *Manufacturing Automation*, 1 ed. Cambridge University Press, New York, NY.

[37] Martelloti, M., 1941. "An analysis of the milling process". *Transactions of the ASME,* **63**, pp. 677–700.

[38] Martelloti, M., 1945. "An analysis of the milling process, part 2: Downmilling". *Transactions of the ASME,* **67**, pp. 233–251.

[39] Mann, B., and Patel, B., 2008. "Stability of delay equations written as state space models". *Journal of vibration and control*. Accepted.

[40] Mann, B. P., and Young, K. A., 2006. "An empirical approach for delayed oscillator stability and parametric identification". *Proceedings of the Royal Society A,* **462**, pp. 2145–2160.

[41] Sims, N., Mann, B., and Huyanan, S., 2008. "Analytical prediction of chatter stability for variable pitch and variable helix milling tools". *Journal of Sound and Vibration,* **317**, pp. 664–686.